# Martin Marietta Laboratories

MARTIN MARIETTA

MML TR 94-02

## ELECTROCHEMICAL BEHAVIOR AND SURFACE CHEMISTRY OF NONEQUILIBRIUM ALUMINUM ALLOYS: PASSIVITY MECHANISM AND FABRICATION METHODS

G.D. Davis,* B.A. Shaw,** B.J. Rees,* A. Iyengar,** and E.L. Principe**

*Martin Marietta Laboratories•Baltimore
Baltimore, Maryland

**Department of Engineering Science and Mechanics
The Pennsylvania State University
University Park, Pennsylvania



Final Report for ONR contract N00014-C-93-0007

January 1994

SECURITY CLASSIFICATION OF THIS PAGE

# REPORT DOCUMENTATION PAGE

| | |
|---|---|
| 1a REPORT SECURITY CLASSIFICATION<br>**Unclassified** | 1b RESTRICTIVE MARKINGS<br>**None** |
| 2a SECURITY CLASSIFICATION AUTHORITY | 3 DISTRIBUTION / AVAILABILITY OF REPORT<br>**Unlimited** |
| 2b DECLASSIFICATION / DOWNGRADING SCHEDULE<br>**None** | |
| 4 PERFORMING ORGANIZATION REPORT NUMBER(S)<br>**MML TR 94-02** | 5 MONITORING ORGANIZATION REPORT NUMBER(S) |
| 6a NAME OF PERFORMING ORGANIZATION<br>**Martin Marietta Corporation**<br>**Martin Marietta Laboratories**<br>**Baltimore**<br>6b OFFICE SYMBOL *(If applicable)* | 7a NAME OF MONITORING ORGANIZATION<br>**Defense Contract Administration Services Management Area - Baltimore** |
| 6c ADDRESS *(City, State, and ZIP Code)*<br>**1450 South Rolling Road**<br>**Baltimore, MD 21227-3898** | 7b ADDRESS *(City, State, and ZIP Code)*<br>**300 East Joppa Road**<br>**Baltimore, MD 21204-3099** |
| 8a NAME OF FUNDING / SPONSORING ORGANIZATION<br>**Office of Naval Research**<br>8b OFFICE SYMBOL *(If applicable)*<br>**ONR** | 9 PROCUREMENT INSTRUMENT IDENTIFICATION NUMBER<br>**N00014-C-93-0007** |
| 8c ADDRESS *(City, State, and ZIP Code)*<br>**800 North Quincy Street**<br>**Arlington, VA 22217-5000** | 10 SOURCE OF FUNDING NUMBERS<br>PROGRAM ELEMENT NO. / PROJECT NO / TASK NO / WORK UNIT ACCESSION NO |
| 11 TITLE *(Include Security Classification)*<br>**Electrochemical Behavior and Surface Chemistry of Nonequilibrium Aluminum Alloys: Passivity Mechanism and Fabrication Methods** | |
| 12 PERSONAL AUTHOR(S)<br>**G.D. Davis, B.A. Shaw, B.J. Rees, A. Iyengar and E.L. Principe** | |
| 13a TYPE OF REPORT<br>**Annual** | 13b TIME COVERED<br>FROM **12/1/92** TO **11/30/93** |
| 14 DATE OF REPORT *(Year, Month, Day)*<br>**1994 January 17** | 15 PAGE COUNT<br>**27** |
| 16 SUPPLEMENTARY NOTATION | |

| 17 COSATI CODES | | |
|---|---|---|
| FIELD | GROUP | SUB-GROUP |
| | | |
| | | |

18 SUBJECT TERMS *(Continue on reverse if necessary and identify by block number)*
**Approved for public release; distribution unlimited. Reproduction in whole or in part is permitted for any purpose of the United States Government**

19 ABSTRACT *(Continue on reverse if necessary and identify by block number)*

**The electrochemical behavior of sputter-deposited nonequilibrium stainless aluminum alloys and different methods to produce bulk or thick-film material have been investigated. Nonquilibrium Al-Ta and Al-W alloys exhibit enhanced passivity over a wide pH range even though the passive film chemistry varies considerably. This enhanced passivity can be explained by the Solute-Rich Interphase Mechanism (SRIM) which states that formation and passivation of occluded cells stabilize the passive film from continued $Cl^-$ attack and dissolution. The best material is produced by sputter deposition, however, physical vapor deposited and plasma sprayed material also exhibit some enhanced passivity.**

| | |
|---|---|
| 20 DISTRIBUTION / AVAILABILITY OF ABSTRACT<br>☐ UNCLASSIFIED/UNLIMITED ☐ SAME AS RPT ☐ DTIC USERS | 21 ABSTRACT SECURITY CLASSIFICATION<br>**Unclassified** |
| 22a NAME OF RESPONSIBLE INDIVIDUAL<br>**Dr. Guy D. Davis** | 22b TELEPHONE *(Include Area Code)*<br>**410-204-2376**<br>22c OFFICE SYMBOL |

DD FORM 1473, 84 MAR 83 APR edition may be used until exhausted
All other editions are obsolete

SECURITY CLASSIFICATION OF THIS PAGE

☆ U.S. Government Printing Office 1986—607-044

# ELECTROCHEMICAL BEHAVIOR AND SURFACE CHEMISTRY OF NONEQUILIBRIUM ALUMINUM ALLOYS: PASSIVITY MECHANISM AND FABRICATION METHODS

G.D. Davis,* B.A. Shaw,** B.J. Rees,* A. Iyengar,** and E.L. Principe**

*Martin Marietta Laboratories•Baltimore
Baltimore, Maryland

**Department of Engineering Science and Mechanics
The Pennsylvania State University
University Park, Pennsylvania

Final Report for ONR contract N00014-C-93-0007

January 1994

## ABSTRACT

The electrochemical behavior of sputter-deposited nonequilibrium stainless aluminum alloys and different methods to produce bulk or thick-film material have been investigated. Nonequilibrium Al-Ta and Al-W alloys exhibit enhanced passivity over a wide pH range even though the passive film chemistry varies considerably. This enhanced passivity can be explained by the Solute-Rich Interphase Mechanism (SRIM) which states that formation and passivation of occluded cells are controlled by localized concentrations of solute. The higher concentrations of solute at the metal-oxide interface and around occluded cells stabilize the passive film from continued $Cl^-$ attack and dissolution. The best material is produced by sputter deposition, however, physical vapor deposited and plasma sprayed material also exhibit some enhanced passivity.

## INTRODUCTION

Aluminum alloys are generally designed for improved mechanical properties which are provided via precipitation hardening. Such precipitates can form microgalvanic couples with the surrounding matrix and lead to accelerated corrosion. Chloride-containing environments also promote localized attack even in pure aluminum. Although the corrosion resistance of steels can be dramatically improved by the incorporation of chromium, molybdenum, and other elements to make stainless steels, there are no equivalent conventional stainless aluminum alloys. The failure to produce such alloys is largely due to the very low solubility of passivating species in aluminum; above a small fraction of an atomic percent, these species form precipitates, and can increase corrosion. Consequently, enhanced passivity requires super-saturated, non-equilibrium alloys.

In the last several years, supersaturated aluminum alloys with Mo, Cr, Ta, W, Zr, Nb, Zn, V, Cu, Ti, and Si have been produced by several groups using rapid solidification or other nonequilibrium methods [1-31], such as sputter deposition [1-10,16-23,28-33], ion implantation [11-15,24,25], melt spinning [27], and vapor deposition [26,33]. Several alloys have shown significant improvements in passivity in chloride-containing environments. For our sputter-deposited thin films, Al-W, Al-Ta, and Al-Mo alloys have shown the best performance with breakdown potentials $E_b$ well above 0 V (SCE) and passive regions exceeding 1000 mV in 0.1 M $Cl^-$ solutions [4-9].

The highest $E_b$ values have been exhibited by sputter deposited material. Such thin film material has potential applications in composite materials and electronic devices. More general applications will require bulk material or, at least, thicker coatings. Accordingly, in addition to further evaluation of passivity mechanisms, we have evaluated (to different extents) two new methods by which thick film coatings would be made: metal-organic chemical vapor deposition (MOCVD) and plasma spray.

In this report, we present the results of these two areas of our investigation and also place the most recent work in perspective with previous findings. Because the mechanism development is a continuation, some of the results have been previously reported [33], but are re-presented to support and explain our mechanism.

## PASSIVITY MECHANISM BACKGROUND

Several different mechanisms have been proposed to explain the passivity of stainless aluminum alloys, including electrostatic repulsion of $Cl^-$ by oxidized solute atoms [1-3], formation of an oxidized solute barrier layer [3,4], blockage of $Cl^-$ transport through the passive film [22], stabilization of the passive film oxide structure [6], replacement of oxidized Al in the passive film by oxidized solute to form a more stable oxide [28,29], reduction of the critical pH for pit propagation [17-20], and reduction in $Cl^-$ adsorption due to $pH_{pzc}$ changes [11-15]. Additionally, Macdonald and coworkers [34,35] studying Mo- and W-containing stainless steels have proposed a solute-vacancy interaction model (SVIM). This model suggests that pits originate as vacancies collect at the metal/passive film interface. This condensation of vacancies

causes the film to collapse locally; highly oxidized solute atoms form complexes with cation vacancies formed by $Cl^-$ adsorption to reduce the diffusivity of the vacancies and slow their buildup at the metal/film interface. Olefjord et al. [36-38] have proposed that general corrosion of stainless steels containing Ni and Mo is reduced by a buildup of the solute at the metal surface that provokes passivity by lowering the dissolution rate of the metal substrate during the active dissolution phase. They postulated that a solute build-up might also occur in the upper atomic layers of the metal during pitting and crevice attack and act in a similar manner [36].

Many of these mechanisms are variations and describe different aspects of the same phenomena. It is also possible that different mechanisms may control the passivity of the various stainless aluminum alloys under different conditions. Recently, we proposed a solute-rich interphase mechanism (SRIM) that incorporates various aspects of several mechanisms to explain the enhanced passivity of Al-W and Al-Ta alloys [9,32]. We have continued to characterize and test stainless aluminum alloys under different conditions to further evaluate the passivity of these alloys and to determine the applicability of this mechanism to other alloys.

The behavior of these alloys at non-neutral pH values is of special interest because of the acidification of the solution in an occluded cell and because the Pourbaix diagrams [39] for W and Ta and the literature for stainless steels suggest that the passivity of Al could be extended outside the pH range of 4 to 9 through the nonequilibrium addition of these elements to Al. The Pourbaix diagrams for Al, W, and Ta reveal that passivity is anticipated at low pH values for W, at neutral pH values for Al, and over the entire range of pH values for Ta. It is reasonable to believe that the passivity of Al could be extended to lower pH values through the nonequilibrium addition of W and Ta and, in fact, this has been demonstrated in 1 M HCl by Yoshioka et al. [28,29] for high-concentration, amorphous nonequilibrium Al alloys. The literature for stainless steels [40-43] has also shown that the addition of W (in the presence of a significant amount of Ni) enhances passivity at low pH values.

## EXPERIMENTAL PROCEDURE

*Thick-Film Production*

Two methods for producing thick films of nonequlibrium alloys were evaluated: metal-organic chemical vapor deposition (MOCVD) and plasma spray. MOCVD was attempted by subliming a mixture of aluminum acetylacetonate and the hexacarbonyl of tungsten, chromium, or molybdenum in closed glassware purged with nitrogen. A silicon wafer was resistively heated to decompose the metal-organic compounds as they collided with the substrate. Each wafer was subsequently cleaved and the material characterized by x-ray diffraction (XRD) and x-ray photoelectron spectroscopy (XPS).

Nine plasma sprayed aluminum-tungsten coatings were produced on cold rolled steel plates (4 x 4 x 0.14 in.) using a Metco 7M plasma spraying system with 4MP dual powder feeders. Prealloyed aluminum-tungsten (99.15%Al-0.85%W) powder and pure tungsten powder were used. Both powders were specified at -200 mesh (+30 m).

The substrates were grit blasted in a Norton arrow blast and preheated, but cooled during spraying. The specifications for these samples are given in Table 1. In this report, W concentrations used to denote samples refer to design values and not actual values as discussed below.

**Table 1: Description of specimens**

| DESIGN COMPOSITION | COATING THICKNESS (in) | COATING DESIGNATION |
|---|---|---|
| Al-40%W | 0.02455 | 40A |
| Al-40%W | 0.01985 | 40B |
| Al-40%W | 0.0369 | 40C |
| Al-25%W | 0.02655 | 25A |
| Al-25%W | 0.02315 | 25B |
| Al-15%W | 0.0280 | 15A |
| Al-15%W | 0.0277 | 15B |
| Al-5%W | 0.0220 | 5A |
| Al-5%W | 0.02495 | 5B |

*Coating characteri ıtion*

All the specimens were observed before and after testing under a low power optical microscope while the cross section of at least one specimen at each sample was observed under a high power optical microscope. Selected specimens were studied under a scanning electron microscope (SEM) before and after the electrochemical testing. Energy dispersive X-ray spectroscopy (EDS) was also conducted on the breakdown sites to identify the elements and to evaluate the extent of damage on the coating. EDS mapping was done of an untested specimen to study the distribution of tungsten and aluminum on the surface.

*Electrochemical tests*

Most of the specimens were tested in a standard EG&G PAR flat cell in 0.1 M sodium chloride solution at an approximate pH of 8.0. Saturated calomel was used as the reference electrode and all potentials are given relative to SCE. Some samples with 5% W were not entirely flat and this led the solution to leak out through the hole at the specimen end of the flat cell. Therefore, these samples were tested in Nalgene containers. The samples were coated with two coats of Interlux marine epoxy paint. Anodic polarization scans were run using the PAR model 352 Softcorr software. The scans were begun at 0.01 V below the open circuit potential and ended at 1.6 - 2.0 V above the open circuit potential. Scans were generally run at 0.2 mV/s because a slower scan rate (0.05 mV/s) did not significantly change the results.

## RESULTS AND DISCUSSION

*MOCVD Material*

MOCVD specimens were examined by XRD and XPS and found to be predominately oxidized material ($Al_2O_3$ and oxidized solute) regardless of alloy. Apparently leakage of oxygen from the atmosphere into the glass reaction vessel was sufficient to oxidize the alloy as it was formed. Attempts were made to eliminate or reduce the leaks, but satisfactory material was not achieved with the limited budget available to pursue this approach. It is believed that the approach warrents further investigation using a vacuum chamber as the reaction vessel.

*Plasma-Sprayed Material*

Analysis of the coatings under the low power optical microscope showed the general rough nature of the surface as is typical of any metal sprayed surface. SEM analysis of the coating surface revealed that there were spherical deposits on the surface which indicated incomplete melting of either W or Al powders. Initially, it was presumed that these deposits were particles of W which had not melted due to the high melting point of W as compared to Al. However, EDS analysis of the particles revealed that these deposits were Al indicating that a few Al particles were not completely melted during the spraying operation. EDS analysis revealed no W (above the detection limit) on either the polarized or unexposed surface. SEM micrographs of the exposed area of one of the specimens are shown in Figure 1. The higher magnification view shows the spherical deposits of Al. Figures 2 and 3 are micrographs showing the deposits of Al in different stages at disintegration. Samples of unmelted W powder were also observed under the SEM to confirm that the deposits were not W. Figure 4 shows that W powder is not as spherical as the Al powder and is of a different size. However, it is not known how melting would change shape and size.

The electrochemical results are presented in Table 2. Virtually no change in breakdown potential was observed with design concentration. The Al-40W specimens had an average breakdown potential of -624 mV and an average passive current density of 9.6 $A/cm^2$. The Al-25W specimens had an average breakdown potential of -626 mV and an average passive current density of 17.8 $A/cm^2$. The Al-15W exhibited an average breakdown potential of -613 mV and an average passive current density of 6.2 $A/cm^2$, while the Al-5W had an average breakdown potential of -633 mV and an average passive current density of 10.2 $A/cm^2$. The similarity in average $E_b$ for the different design concentrations reflects the failure to incorporate the W powder into the coating. On the other hand, the values are consistantly higher than that of pure aluminum (-690 mV) reflecting the W prealloyed into the powder.

Figures 5-8 show replicate anodic polarization scans of the Al-40W, Al-25W, Al-15W and Al-5W specimens respectively. Anodic polarization scans of the specimens with varying design W concentrations overlaid on each other are shown in Figure 9. These figures illustrate the variability in $E_{oc}$ and $i_p$ and the greater consistency in $E_b$.

**Table 2. Electrochemical Behavior of Plasma Sprayed Specimens**

| File Name | Composition | $E_{OC}$ (mV) | Scan Rate (mV/s) | $E_b$ (mV) | $i_p$ A/cm$^2$ |
|---|---|---|---|---|---|
| 40A1 | Al-40W | -718 | 0.2 | -624 | 16.1 |
| 40A2 | Al-40W | -678 | 0.2 | -623 | 2.3 |
| 40A3 | Al-40W | -665 | 0.05 | -636 | 18 |
| 40BI | Al-40W | -754 | 0.2 | -619 | 18.4 |
| 40B2 | Al-40W | -680 | 0.2 | -597 | 16.8 |
| 40B3 | Al-40W | -679 | 0.05 | -627 | 0.4 |
| 40CI | Al-40W | -879 | 0.2 | -638 | 7.1 |
| 40C2 | Al-40W | -655 | 0.2 | -598 | 1.8 |
| 40C3 | Al-40W | -812 | 0.05 | -650 | 5.5 |
| 25AI | Al-25W | -839 | 0.2 | -635 | 36 |
| 25A2 | Al-25W | -654 | 0.2 | -596 | 19.2 |
| 25A3 | Al-25W | -658 | 0.05 | -651 | 17.6 |
| 25BI | Al-25W | -757 | 0.2 | -640 | 11 |
| 25B2 | Al-25W | -833 | 0.2 | -613 | 5.2 |
| 25B3 | Al-25W | -661 | 0.05 | -619 | 17.6 |
| 15AI | Al-15W | -737 | 0. 2 | -637 | 7.9 |
| 15A2 | Al-15W | -686 | 0.2 | -568 | 2.6 |
| 15A3 | Al-15W | -661 | 0.05 | -620 | 2.6 |
| 15BI | Al-15W | -792 | 0.2 | -622 | 19.4 |
| 15B2 | Al-15W | -758 | 0.2 | -612 | 3.6 |
| 15B3 | Al-15W | -678 | 0.05 | -620 | 0.9 |
| 5A1 | Al-5W | -694 | 0.2 | -666 | 2.9 |
| 5A2 | Al-5W | -702 | 0.2 | -641 | 0.8 |
| 5A3 | Al-5W | -799 | 0.05 | -626 | 11.6 |
| 5B1 | Al-5W | -699 | 0.2 | -623 | 19.4 |
| 5B2 | Al-5W | -701 | 0.2 | -618 | 11.9 |
| 5B3 | Al-5W | -671 | 0.05 | -626 | 14.8 |

Figure 9 shows that $E_{OC}$s of the plasma-sprayed alloys have been increased over pure Al reflecting the small amount of W in the samples from the prealloyed Al-W powde: that was not detected by EDS. However, although $E_{OC}$ exhibits considerable scatter, the average $E_{OC}$ is independent of design concentration. Significant variations in $E_{oc}$ for Al and Al alloys in aerated solutions are common. For our specimens, variations in interconnected porosity in the coating may also contribute to the scatter noted. This interconnected porosity in a coating provides a path for the electrolyte to reach the substrate. Thus, porosity variations could influence the open circuit potential. In the cases where $E_{OC}$ is close to that of steel (-660 mV), high porosity may have allowed the substrate to be exposed to the electrolyte. The surface roughness and interconnected porosity increase the exposed surface area and may help explain why the passive current densities for these plasma sprayed samples are high when compared to the sputter-deposited samples that we have tested previously.

The anodic polarization scans of the specimens have been overlaid with a cathodic polarization scan for steel in Figures 10-13. The anodic scan of bulk pure Al has been shown in all the figures and it is quite evident that there is an improvement in the performance of the plasma sprayed coatings over Al. The cathodic scan of steel intersects the pure Al in the breakdown region whereas it intersects the Al-W specimens in the passive/quasi-passive region, thus keeping the corrosion rate to a controlled value. In some cases, the $E_{OC}$s of the Al-W specimens were raised to values above the $E_{OC}$ of the steel. This is to be avoided in coating applications to keep the substrate from undergoing severe corrosion at defects sites in the coating. However, it is beneficial for the $E_{OC}$ of the coatings to be raised to values which are close to that of the substrate. It would also be of great use to lower the passive currents of the Al-W samples further, making the curves intersect at the $E_{OC}$ of the steel. Both these effects would reduce corrosion.

Some specimens did intersect the curve for the steel at $E_{OC}$ while being anodic to the steel. However, these do not show much passivity thus making it a highly unstable condition. In some cases the anodic polarization curves seen were very similar to that which would be expected for steel. It seems from the behavior that the porosity in the coating allowed the electrolyte to reach the steel substrate.

Because porosity plays such an important role in the electrochemical behavior of the plasma sprayed material, we produced a limited number of Al-Ti coatings using the high velocity oxy-fuel process which should minimize coating porosity. Unfortunately, the one attempt did not incorporate much Ti into the coating and the results were not very good.

The $E_b$'s obtained from the plasma sprayed coatings were not as good as those from our sputter-deposited films or even those of our physical vapor-deposited coatings [32,33] (Fig. 14). Nonetheless, they did show improvements in $E_b$ relative to pure Al despite the limited amount of W incorporated into the material. As a result, they are sufficiently encouraging to justify further research in the area using continuing funds available to Penn State University in an attempt to improve and optimize the fabrication process. Further reductions in the passive currents of the alloy would open up a wide area of applications as would increases in the breakdown potentials.

*Passivity Mechanism*

To explain the enhanced passivity of Al-W and Al-Ta alloys over a wide range of pH values despite large changes in the composition of the passive film, we have introduced the solute-rich interphase mechanism [9,32]. The SRIM requires that the film exhibit passivity in the low-pH environment of an occluded cell or protopit. In this mechanism, localized increases in the solute concentration at the metal-oxide interphase and at defects inhibit pit initiation and stabilize the occluded cells that do form. If a defect in the passive film extends to the interphase, the solute-rich metal region (formed during the preferential oxidation of Al in the atmosphere or near-neutral electrolytes) inhibits pit formation by reducing Al dissolution, forming an oxidized solute barrier layer, and reducing $Cl^-$ adsorption by locally reducing the $pH_{pzc}$ (Fig. 15). If Al dissolution and acidification begin, the local solute concentration in both the

alloy and passive film increases further (Fig. 15). The oxidized solute (a combination of $WO_2$ and $WO_3$ or, more likely based on quantitative XPS, $W(OH)_4$ and $W(OH)_6$) is more stable in the low pH environment of the pit than the original film, and the solute repassivates the site. Passivity is further enhanced because, according to the $pH_{pzc}$ mechanism [11-15], less $Cl^-$ would adsorb locally.

The SRIM appears applicable in the Al-Ta case as well. The evolution of the passive film chemistry in the surface behavior diagram (SBD) [44,45] of Figure 16 [33] indicates that this mechanism can indeed explain the enhanced passivity of Al-Ta alloys. The pH 3 data show that $Ta(OH)_5$, a hydrated form of oxidized Ta, is the passivating species under these conditions. As the specimen is polarized, the passive film evolves directly toward $Ta(OH)_5$ (path c) as this species replaces the original oxidized Al. In deaerated pH 8 solutions, the passive film initially is a mixture of partially hydrated $Al_2O_3$ and $Ta_2O_5$, both of which are stable species under these near-neutral conditions. Little change in the composition is noted until $E_b^{Al}$ is approached and the amount of $Ta_2O_5$ increases two-fold. Once $E_b^{Al}$ is exceeded and the alloy exhibits its enhanced passivity, the amount of $Ta(OH)_5$ increases as it replaces the $Ta_2O_5/Al_2O_3$ in the occluded cells and they passivate.

The SRIM predicts that increasing amounts of oxidized solute would be found in the passive film with greater overpotential as the density of repassivated pits increases. This phenomenon of increasing oxidized solute was observed with the Al-W alloys for which the mechanism was developed and is universal in the nonequilibrium aluminum alloys we have investigated [1-9]. Nonetheless, it may not be the only reason for the concentration of oxidized solute to increase and thus the increase in repassivated pit density may not explain all the changes in passive film chemistry during polarization. For example, the increase in $Ta_2O_5$ concentration in the deaerated pH 8 solution prior to $E_b^{Al}$ (Figure 16) is not a result of pit repassivation. On the other hand, the increase in oxidized W concentration as $E_b$ is approached in pH 8 solutions [7] is likely to result from repassivated pits.

The SRIM also predicts an enrichment of solute in the metallic side of the interphase. This increase in metallic concentration was first observed in the Al-Mo and Al-Cr systems as dealloying and the formation of elemental solute just below the passive film [2,3]. It is also observed for the Al-W and Al-Ta systems as illustrated in Figure 17 for Al-Ta which shows the enrichment to increase with overpotential.

The SRIM explains why mechanisms involving properties of an oxidized solute passive film, such as barrier layer formation [1-4,22,28,29], $pH_{pzc}$ reduction [11-15], and solubility reduction in low-pH environments [17-20], can appear to account for the enhanced passivity of these alloys despite the fact that the passive film is at least half oxidized or hydrated aluminum and can be almost entirely oxidized or hydrated aluminum, depending on the alloy system and the polarization conditions. The important factor is the solute's localized concentration at the interphase and in occluded cells, not the overall concentration of the solute in the passive film. For example, the mechanism explains the correlation of $E_b$ with the $pH_{pzc}$ of the oxidized solute [15] despite the wide range of solute concentration in the passive film seen for

different alloys under different conditions. Because the film in an occluded cell is predominately oxidized solute, the local $pH_{pzc}$ would be considerably lower than that of the passive film away from a cell and would be close to that of the oxidized solute. Likewise, a barrier layer oxide, regardless of process by which it acts as a barrier, is needed most where attack is occurring. Thus a local barrier layer can be nearly as effective against pitting as a barrier layer that is present over the entire surface. Finally, the increased low-pH stability of the oxidized solute in an occluded cell reduces solubility of the local passive film. The resulting decreased acidification of the local environment diminishes the tendency of the cell to grow as postulated by Smialowska [18-20] and further developed by Frankel et al. [17].

Olefjord and coworkers [36-38] have also reported an enrichment of the solute in stainless steels during the active dissolution stage because of preferential dissolution of iron. This enrichment provokes passivation by lowering the dissolution rate in the active phase and controlling the electrochemical behavior of the alloy. They demonstrated this effect for the general corrosion of Cr-Ni-Mo alloyed steels and showed that synergistic effects between the enriched solute elements control the formation of the passive film and other electrochemical reactions. They went on to speculate that similar solute enrichments in the outer regions of the metal might also improve resistance to pitting and crevice corrosion. This hypothesis is consistent with our SRIM mechanism.

Because the SRIM incorporates aspects of mechanisms proposed by several different groups for a variety of alloys, it may be more universal than the Al-W and Al-Ta alloys to which we have applied it. Nonetheless, it does require that the solute forms a more protective passivating species than Al or induces a synergistic stabilization of Al, especially under conditions within occluded cells. Such species could be inherently more thermodynamically stable as indicated by Pourbaix diagrams or more stable in a kinetic sense that dissolution reactions proceed much more slowly.

## CONCLUSIONS

The best nonequilbirium material is produced by sputter deposition. Thicker material can be produced by plasma spraying or by physical vapor deposition, as reported in a previous report [33], but the degree of enhanced passivity is not as great as that observed for the sputter deposited material. Nonetheless, it may prove adequate for a number of applications if the deposition process is developed further and optimized. The solute-rich interphase mechanism (SRIM) can explain the enhanced passivity of the Al-Ta and Al-W alloys and possibly other alloys as well. The SRIM provides for the solute in both the metallic and oxidized forms to concentrate at regions of localized attack thus enhancing the passivity of the alloy even when the solute is present in low concentrations.

## REFERENCES

1. W.C. Moshier, G.D. Davis, J.S. Ahearn, and H.F. Hough, *J. Electrochem. Soc.* **133**, 1063 (1986).

2. W.C. Moshier, G.D. Davis, J.S. Ahearn, and H.F. Hough, *J. Electrochem. Soc.* **134**, 2677 (1987).
3. W.C. Moshier, G.D. Davis, and G.O. Cote, *J. Electrochem. Soc.* **136**, 356 (1989).
4. G.D. Davis, W.C. Moshier, T.L. Fritz, and G.O. Cote, *J. Electrochem. Soc.* **137**, 422 (1990).
5. B.A. Shaw, T.L. Fritz, G.D. Davis, and W.C. Moshier, *J. Electrochem. Soc.* **137**, 1317 (1990).
6. G.D. Davis, W.C. Moshier, G.G. Long, and D.R. Black, *J. Electrochem. Soc.* **138**, 3194 (1991).
7. B.A. Shaw, G.D. Davis, T.L. Fritz, B.J. Rees, and W.C. Moshier, *J. Electrochem. Soc.* **138**, 3288 (1991).
8. B.A. Shaw, G.D. Davis, T.L. Fritz, B.J. Rees, and W.C. Moshier, in *Critical Factors in Localized Corrosion*, G.S. Frankel and R.C. Newman, eds. (The Electrochemical Society, Pennington, NJ, 1992), p. 323.
9. G.D. Davis, B.A. Shaw, B.J. Rees, and M. Ferry, *J. Electrochem. Soc.* **140**, 951 (1993).
10. T.R. Schrecengost, B.A. Shaw, and R.G. Wendt, W.C. Moshier, *Corros.* **49**, 842 (1993).
11. P.M. Natishan, E. McCafferty, and G.K. Hubler, *J. Electrochem. Soc.* **133**, 1061 (1986).
12. E. McCafferty, G.K. Hubler, P.M. Natishan, P.G. Moore, R.A. Kant, and B.D. Sartwell, *Mater. Sci. Eng.* **86**, 1 (1987).
13. P.M. Natishan, E. McCafferty, and G.K. Hubler, *J. Electrochem. Soc.* **135**, 321 (1988).
14. P.M. Natishen, E. McCafferty, and G.K. Hubler, *Corros. Sci.* **32,** 721 (1991).
15. E. McCafferty and P.M. Natishan, in *Critical Factors in Localized Corrosion*, G.S. Frankel and R.C. Newman eds. (The Electrochemical Society, Pennington, NJ, 1992), p. 299..
16. G.S. Frankel, M.A. Russak, C.V. Jahnes, M. Mirzamaani, and V.A. Brusic, *J. Electrochem. Soc.* **136**, 1243 (1989).
17. G.S. Frankel, R.C. Newman, C.V. Jahnes, and M.A. Russak, *J. Electrochem. Soc.* **140**, 2192 (1993).
18. Z. Szklarska-Smialowska, in *Critical Factors in Localized Corrosion*, G.S. Frankel and T.C. Newman, eds. (The Electrochemical Society, Pennington, NJ, 1992), p. 311.
19. Z. Szklarska-Smialowska, *Corros. Sci.* **33**, 1193 (1992).
20. R.B. Inturi and Z. Szklarska-Smialowska, *Corros. Sci.* **34**, 1201 (1993).
21. R.C. Bhardwaj, A. González-Martín, and J. O'M. Bockris, *J. Electrochem. Soc.* **139**, 1050 (1992).
22. J. O'M. Bockris and Lj. V. Minevski, *J. Electroanal. Chem.* **349**, 375 (1993).
23. A. González-Martín, R.C. Bhardwaj, and J. O'M. Bockris, accepted by *J. Electrical Anal. Chem.*
24. A.H. Al-Saffar, V. Ashworth, A.K.O. Vairamov, D.J. Chivers, W.A. Grant, R.P.M. Procter, *Corros. Sci.* **20,** 127 (1980).
25. M.V. Zeller and J.A. Kargol, *Appl. Surf. Sci.* **18**, 63 (1984).
26. R.W. Gardiner and M.C. McConnell, *Met. Mater.* **3**, 254 (1987)
27. M. Fass, D. Itzhak, D. Eliezer, F.H. Froes, *J. Mater. Sci. Lett.* **6**, 1227 (1987).
28. H. Yoshioka, H. Habazaki, A. Kawashima, K. Asami, and K. Hashimoto, *Corros. Sci.* **32**, 313 (1991).

29. H. Yoshioka, A. Kawashima, K. Asami, and K. Hashimoto, in *Proc. Symp. Corrosion, Electrochemistry, and Catalysis of Metallic Glasses* R.B. Diegle and K. Hashimoto, eds. (The Electrochemical Society, Pennington, NJ 1988) p. 242.
30. F.G. Schenk, "The Influence of Heat Treatment on the Performance of Highly Corrosion Resistant Al Alloys," Trident Scholar Report No. 197, U.S. Navy Academy, 1992.
31. C.C. Streinz, "A Microellipsometric Study of the Passive Film Formation on Solid Solution Al-Ta Alloys and the Role of $Al_3Ta$ Precipitates in Breakdown," Ph.D. dissertation for The Johns Hopkins University, Baltimore, MD (1992).
32. E.L. Principe, B.A. Shaw, C.A. Pecile, A.S. Iyengar, G.D. Davis, and B.J. Rees, "Nonequilibrium Alloying Studies on Passivity in Chloride Environments," in *Proc. 12th Internat. Corrosion Congr.* (NACE, Houston, TX, 1993), p. 2187.
33. G.D. Davis, B.A. Shaw, B.J. Rees, E.L. Principe, C.A. Pecile, and A.S. Iyengar. Annual Report to ONR on contract N00014-85-C-0638, MML TR 93-04, submitted by Martin Marietta Laboratories, March 1993.
34. M. Urguidi and D.D. Macdonald, *J. Electrochem. Soc.* **132**, 555 (1985)
35. D.D. Macdonald, *J. Electrochem. Soc.* **139**, 3434 (1992).
36. I. Olefjord, *Mater. Sci. Engr.* **42**, 161 (1980).
37. I. Olefjord and B.-O. Elfstrom, *Corros.* **38**, 46 (1982).
38. I. Olefjord, B. Brox, and U. Jelvestrom, *J. Electrochem. Soc.* **132**, 2854 (1985).
39. M. Pourbaix, *Atlas of Electrochemical Equilibria in Aqueous Solutions*, (NACE, Houston, TX 1974) p. 168.
40. N. Bui, A. Irhzo, F. Dabosi, and Y. Limouzin-Maire, *Corros.* **39**, 491 (1983).
41. A. Irhzo, Y. Segui, N. Bui, and F. Dabosi, *Corros. Sci.* **26**, 769 (1986).
42. H. Habazaki. A. Kawashima, Kasami, and K. Hashimoto, in *The Applications of Surface Analysis Methods to Environmental/Material Interactions* (PV 91-7) D.R. Baer, C.R. Clayton, and G.D. Davis, eds., (The Electrochemical Society, Pennington, NJ, 1991) p. 467.
43. J. Chen and J.K. Wu, *Corros. Sci.* **30**, 53 (1990).
44. G.D. Davis, *Surf. Interface Anal.* **9**, 421 (1986).
45. G.D. Davis, T.S. Sun, J.S. Ahearn, and J.D. Venables, *J. Mater. Sci.* **17**, 1807 (1982).

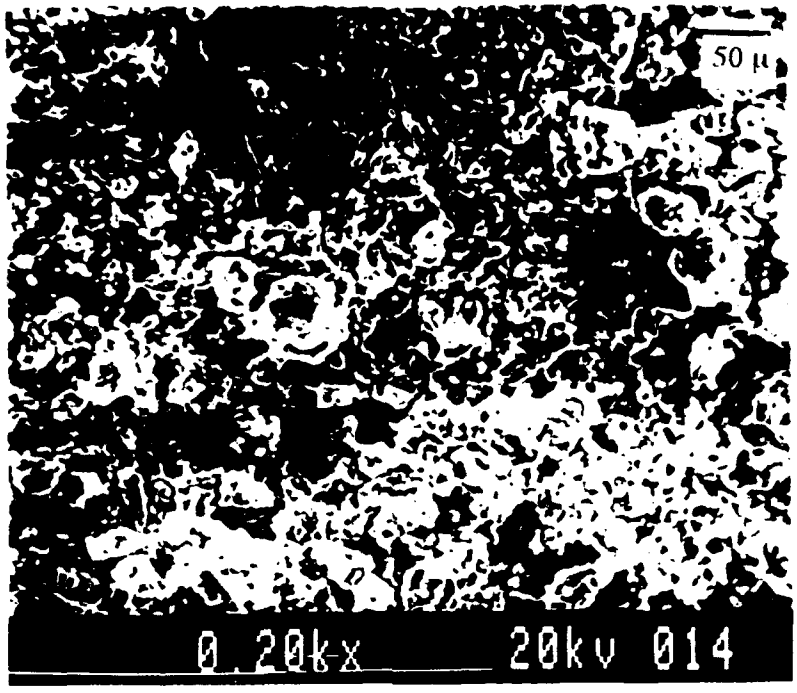


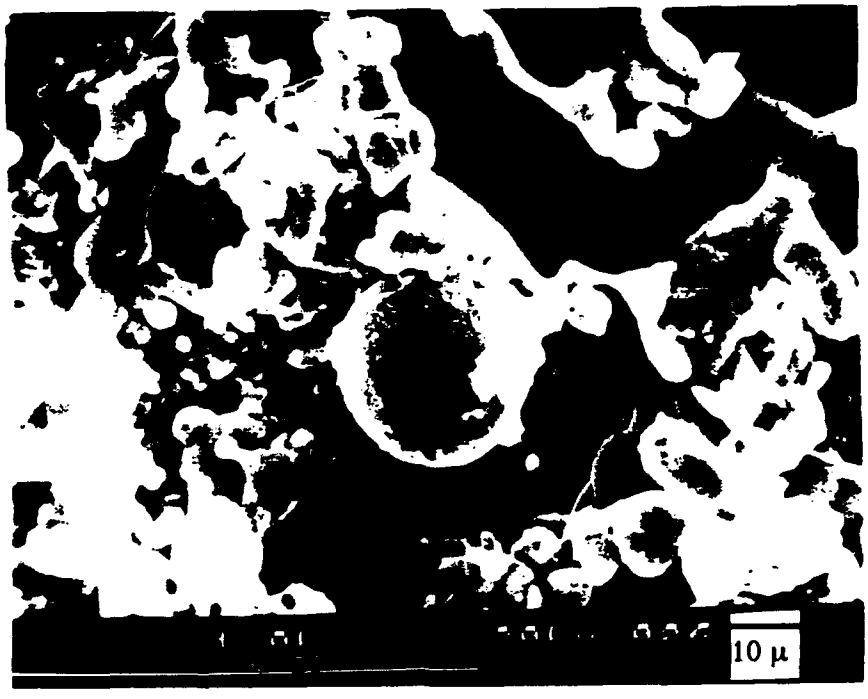


1. a) Micrograph showing the general nature of the sprayed surface after testing. The dark regions on the specimen are believed to be breakdown sites. b) Micrograph showing spherical deposits of Al. The upper right corner illustrates the splat quenched structure desired.

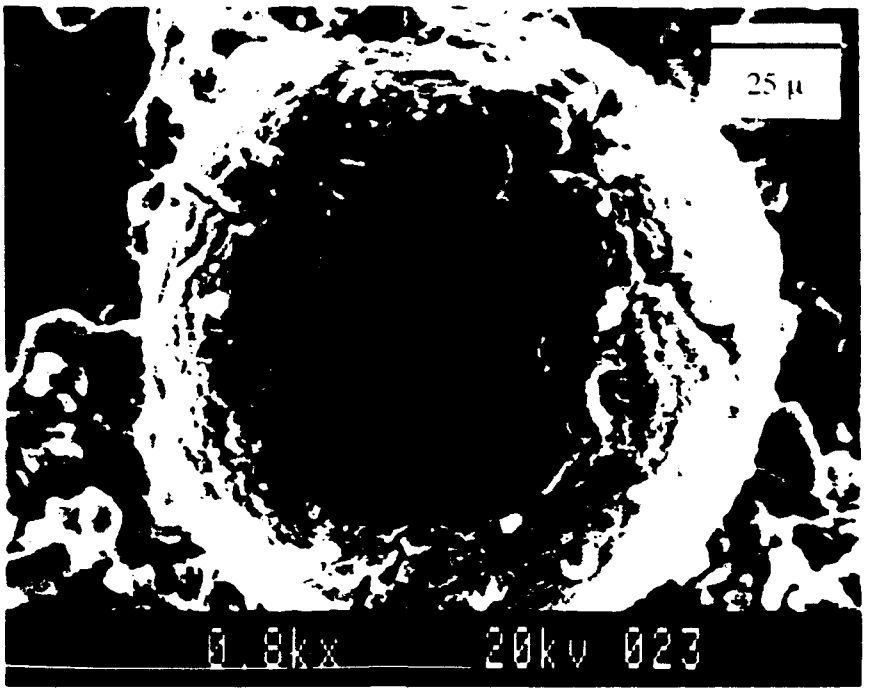


2. The spherical deposits of Al are illustrated at a higher magnification in this micrograph. The particle seems to be disintegrating but not sufficiently to obtain a splat quenched structure.

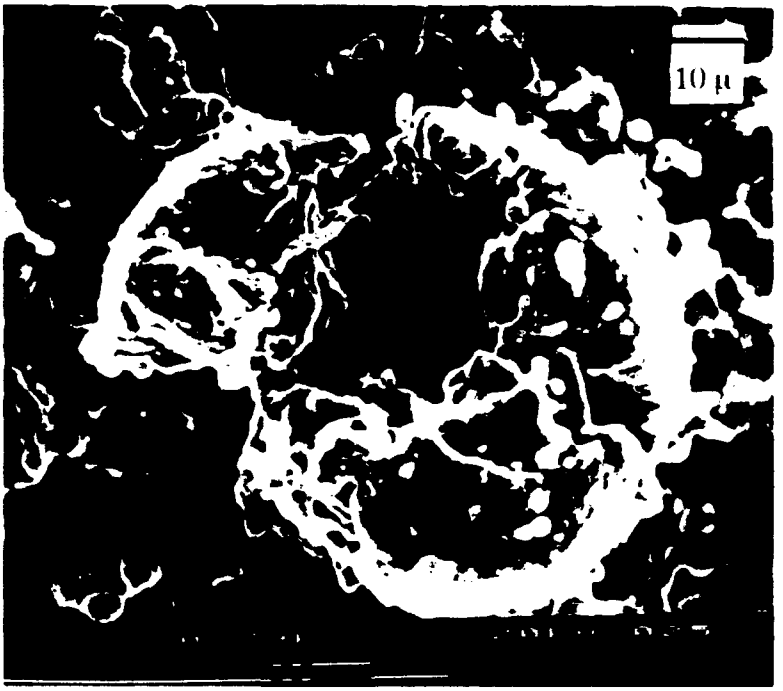


3. Micrograph showing a particle of Al which has disintegrated more than the particle in Figure 2.

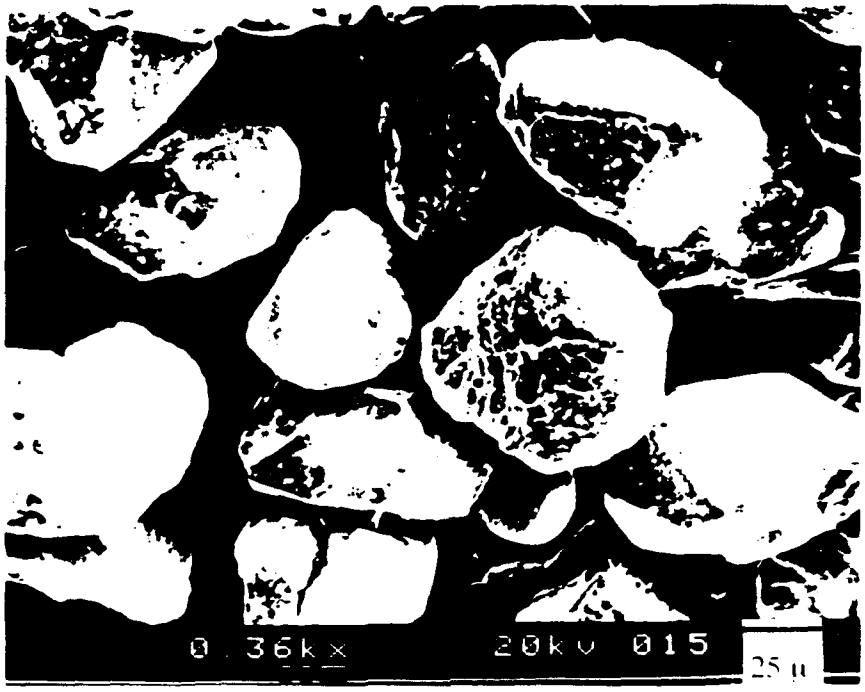


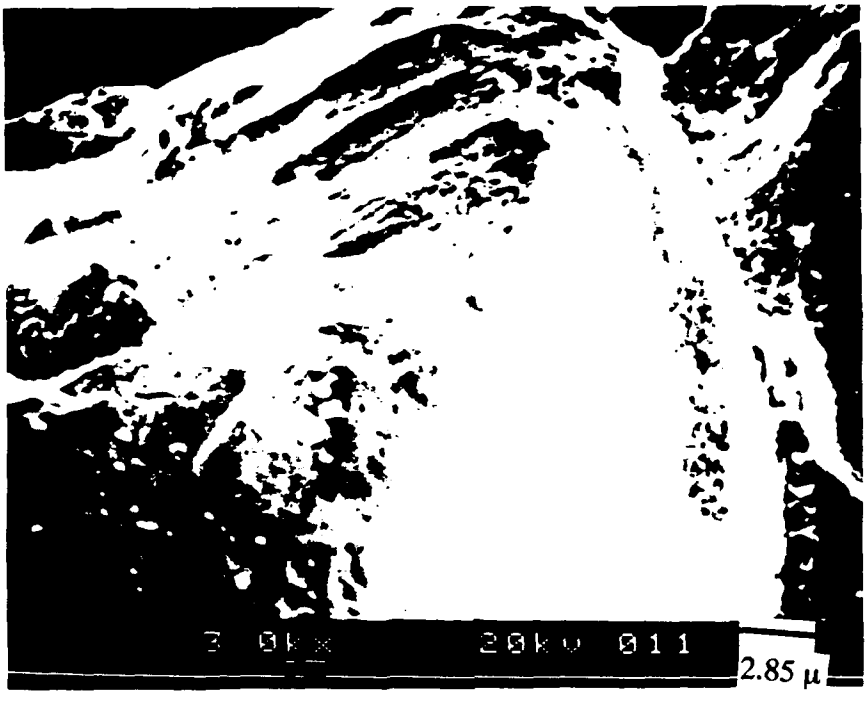


4. Micrographs showing W powder. The W powder is different in shape and size as compared to the deposits seen on the specimen.

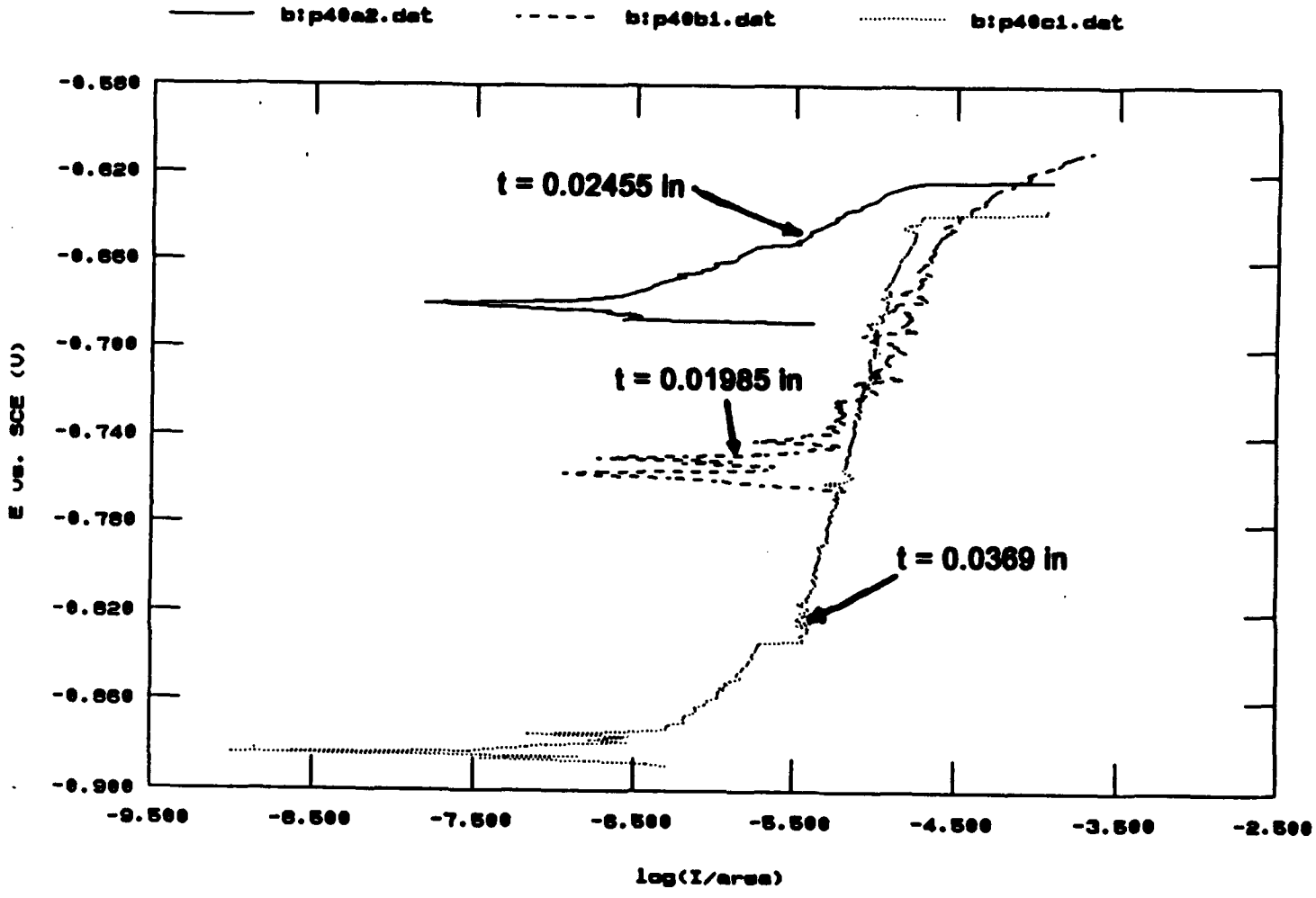


5. Anodic polarization curves generated in 0.1 M NaCl at a scan rate of 0.2 mV/s showing typical variability in performance between three Al40%W coatings. Coating thickness for each panel is noted.

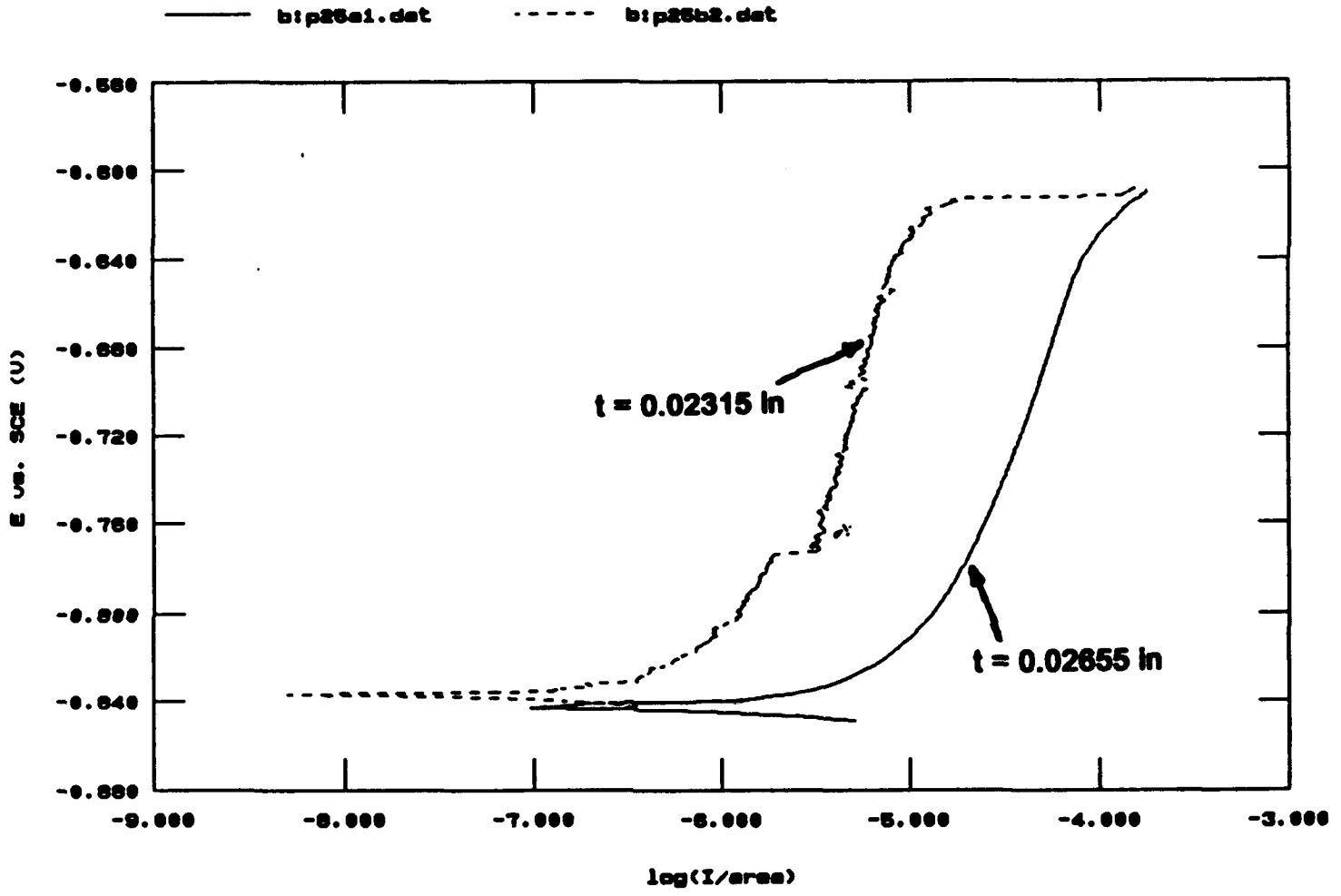


6. Anodic polarization curves generated in 0.1 M NaCl at a scan rate of 0.2 mV/s showing typical variability in performance between two Al25%W coatings. Coating thickness for each panel is noted.

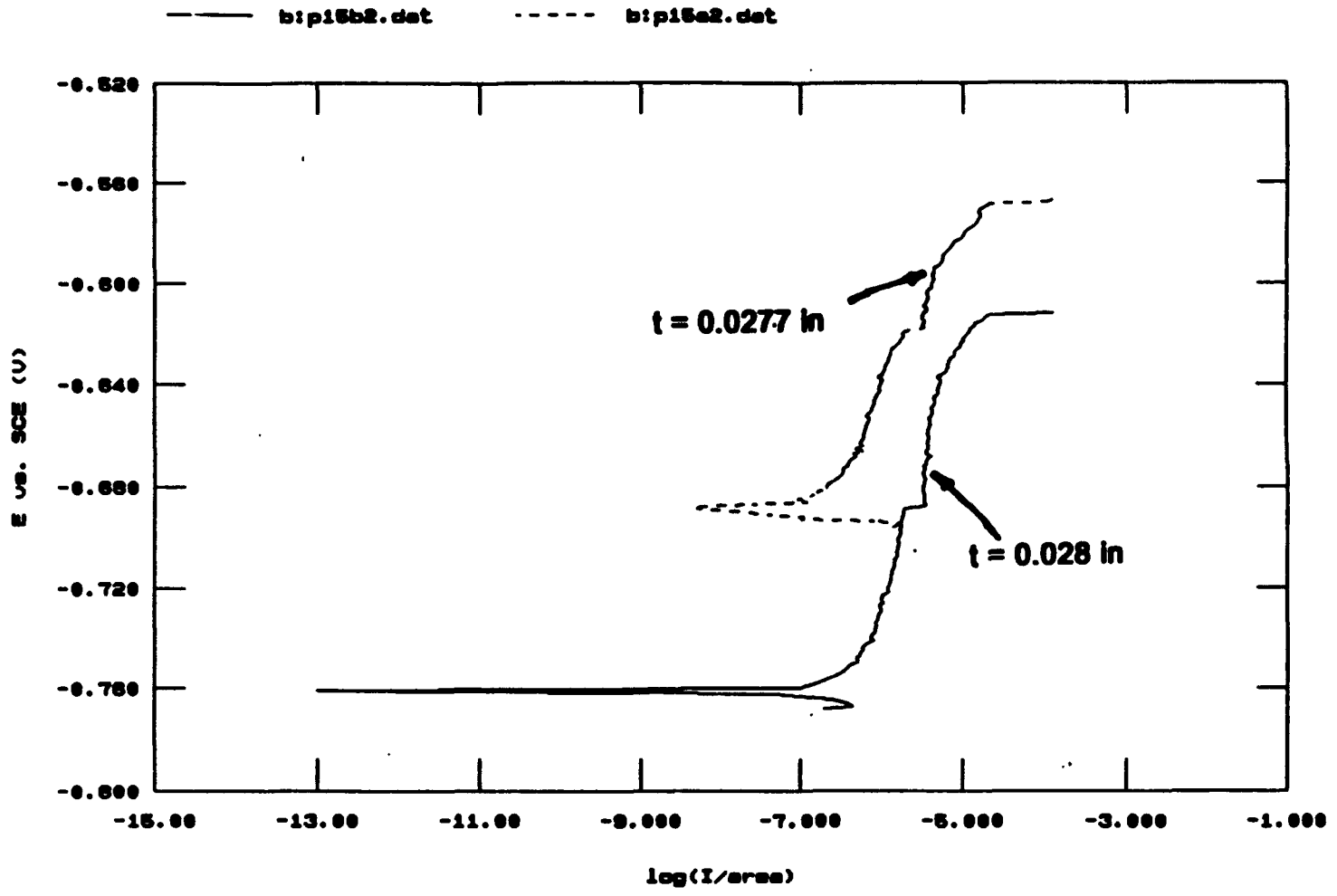


7. Anodic polarization curves generated in 0.1 M NaCl at a scan rate of 0.2 mV/s showing typical variability in performance between two Al15%W coatings. Coating thickness for each panel is noted.

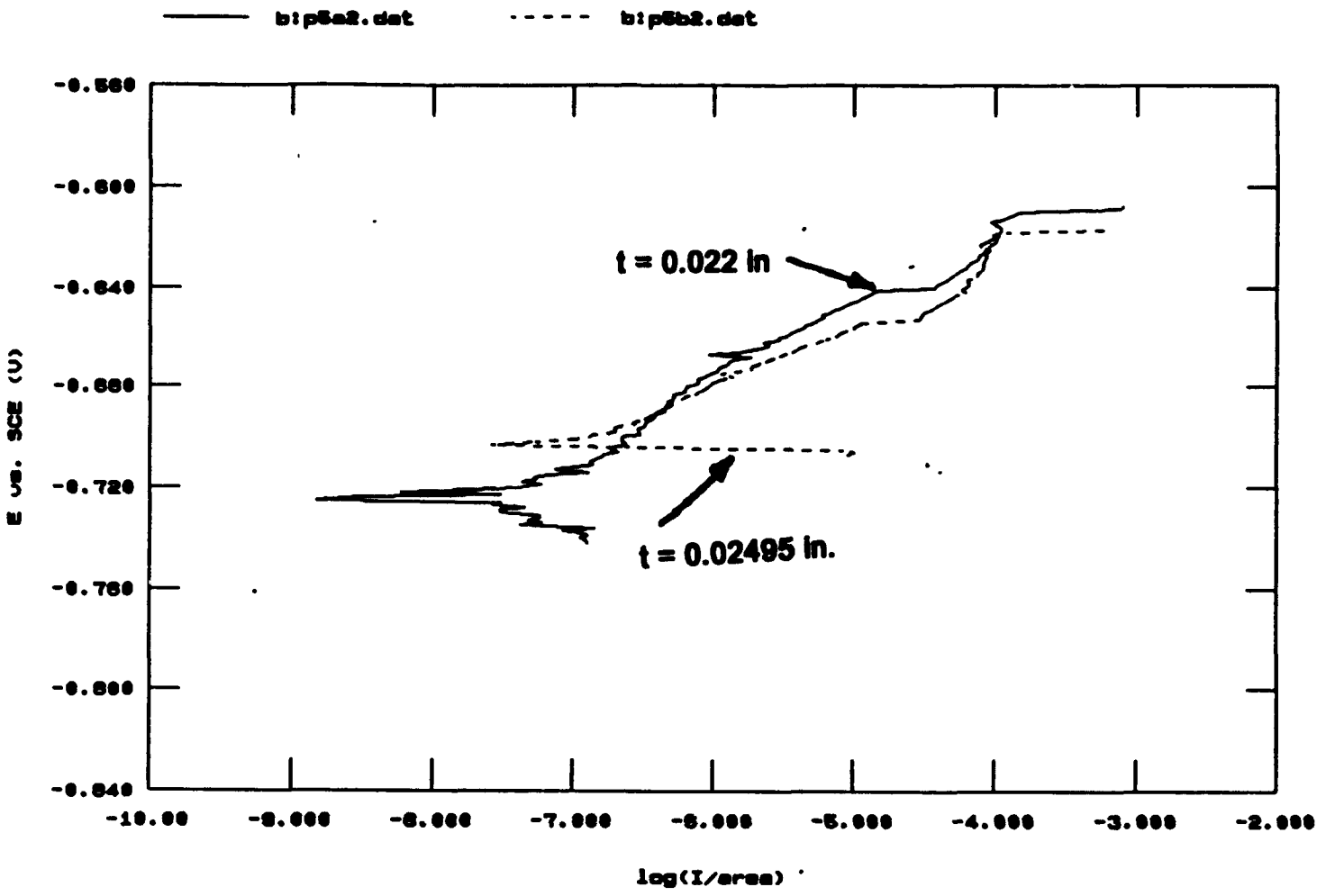


8. Anodic polarization curves generated in 0.1 M NaCl at a scan rate of 0.2 mV/s showing typical variability in performance between two Al5%W coatings. Coating thickness for each panel is noted.

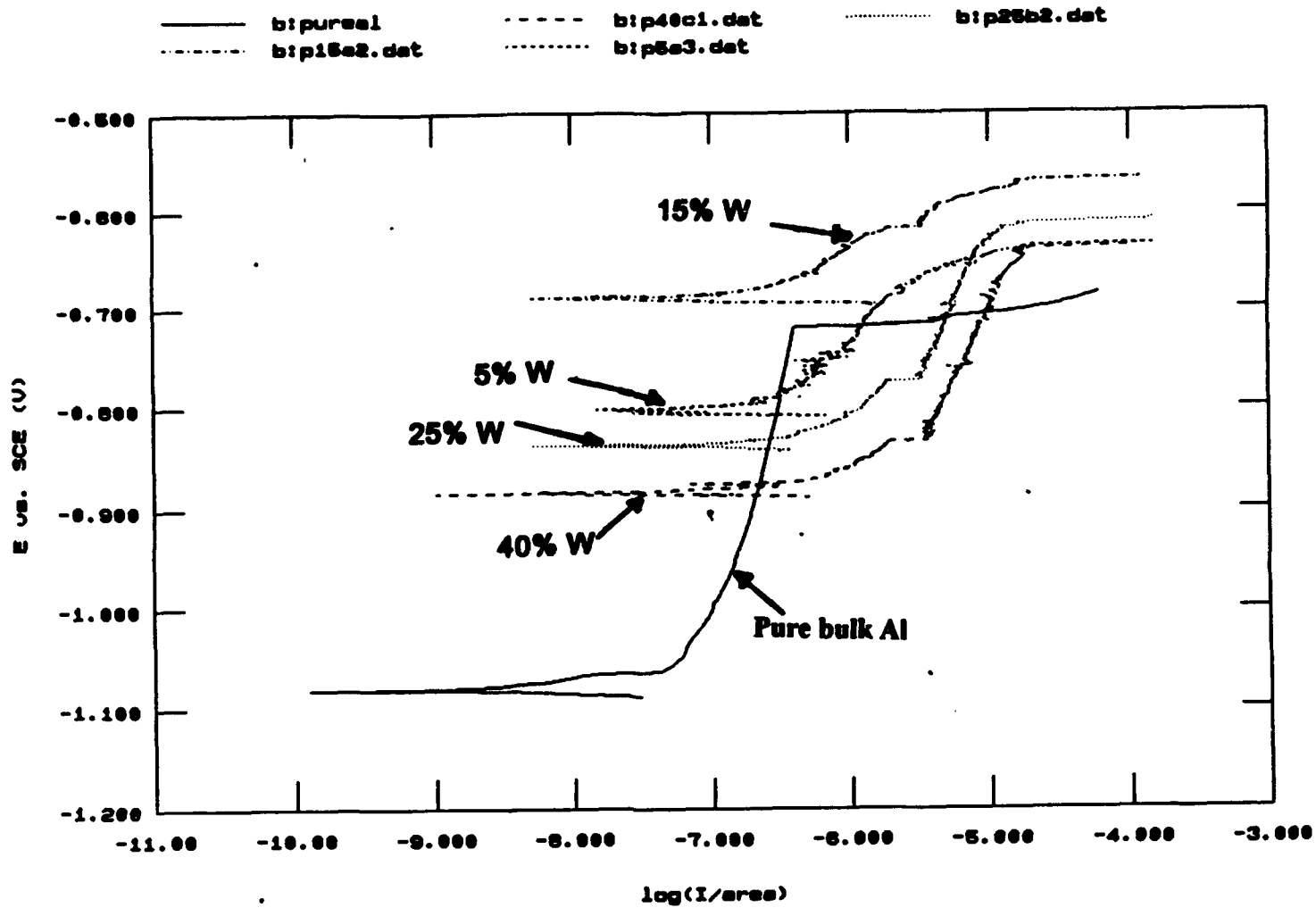


9. Anodic polarization curves of Al-W specimens with different concentrations of W in the powder feeder compared with pure bulk Al. All the scans were run in 0.1 M NaCl at a pH of 8.0.

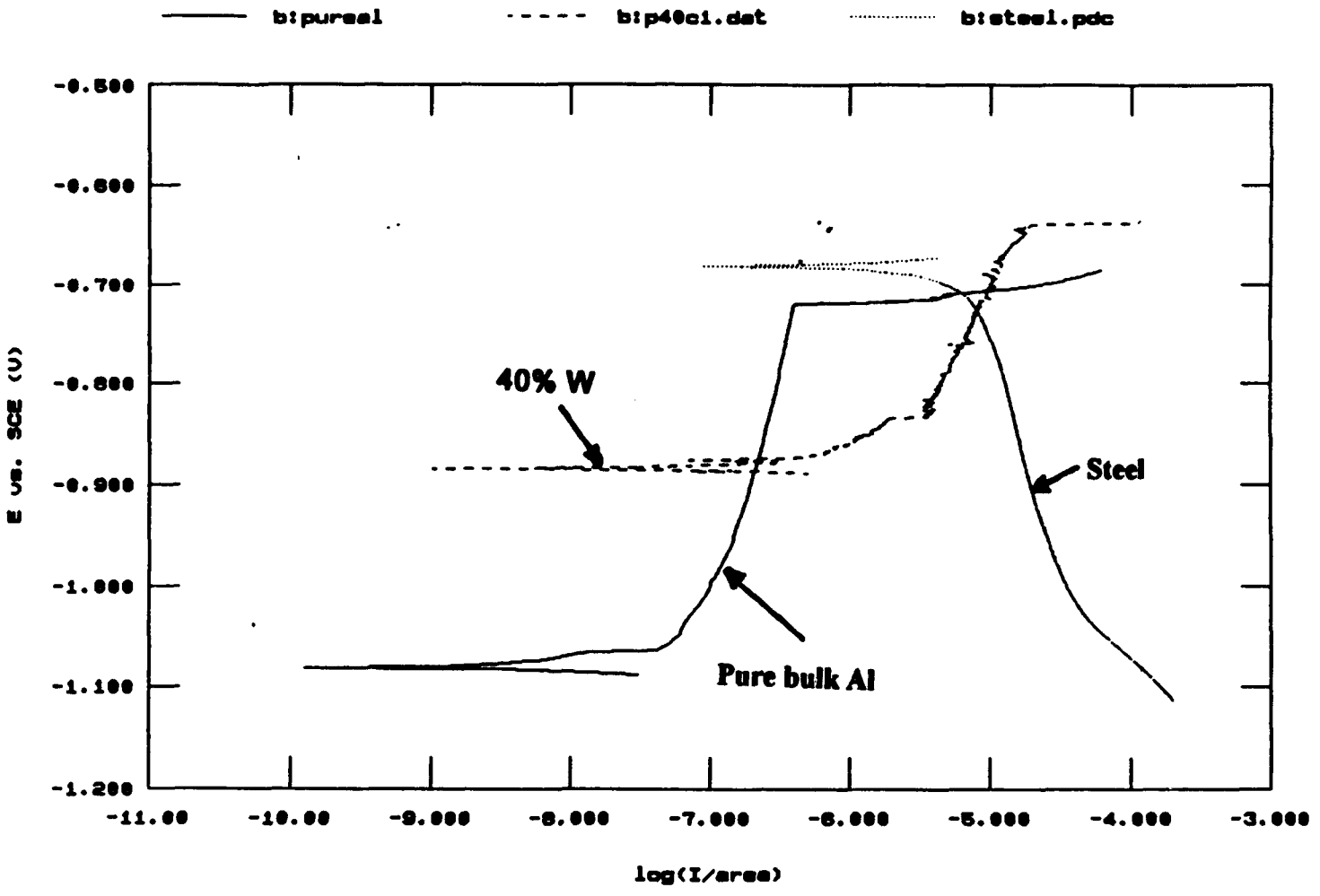


10. Anodic polarization curves of an Al40%W specimen and a pure Al specimen overlaid on the cathodic polarization curve of steel. Both scans were run in 0.1 M NaCl.

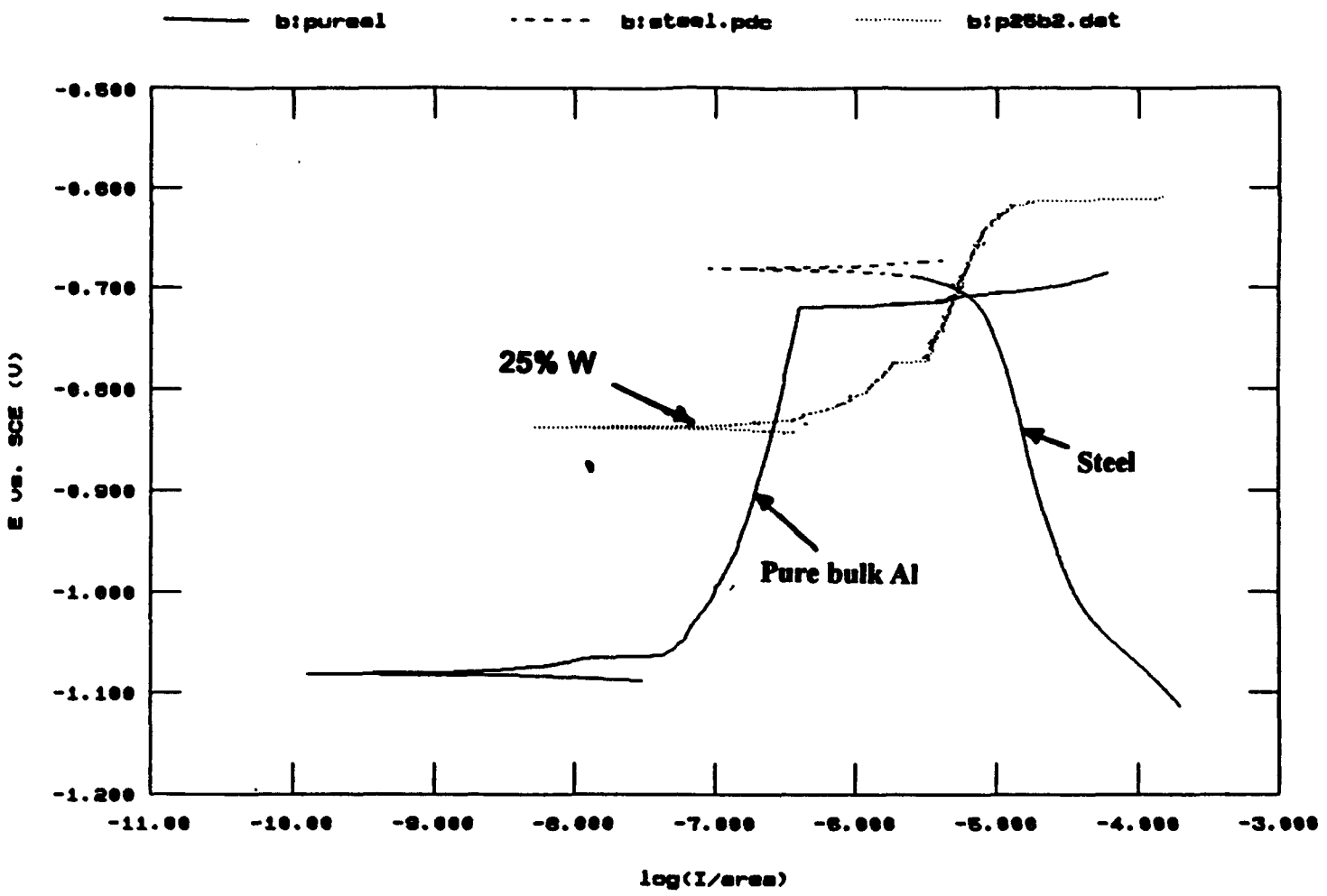


11. Anodic polarization curves of an Al25%W specimen and a pure Al specimen overlaid on the cathodic polarization curve of steel. Both scans were run in 0.1 M NaCl.

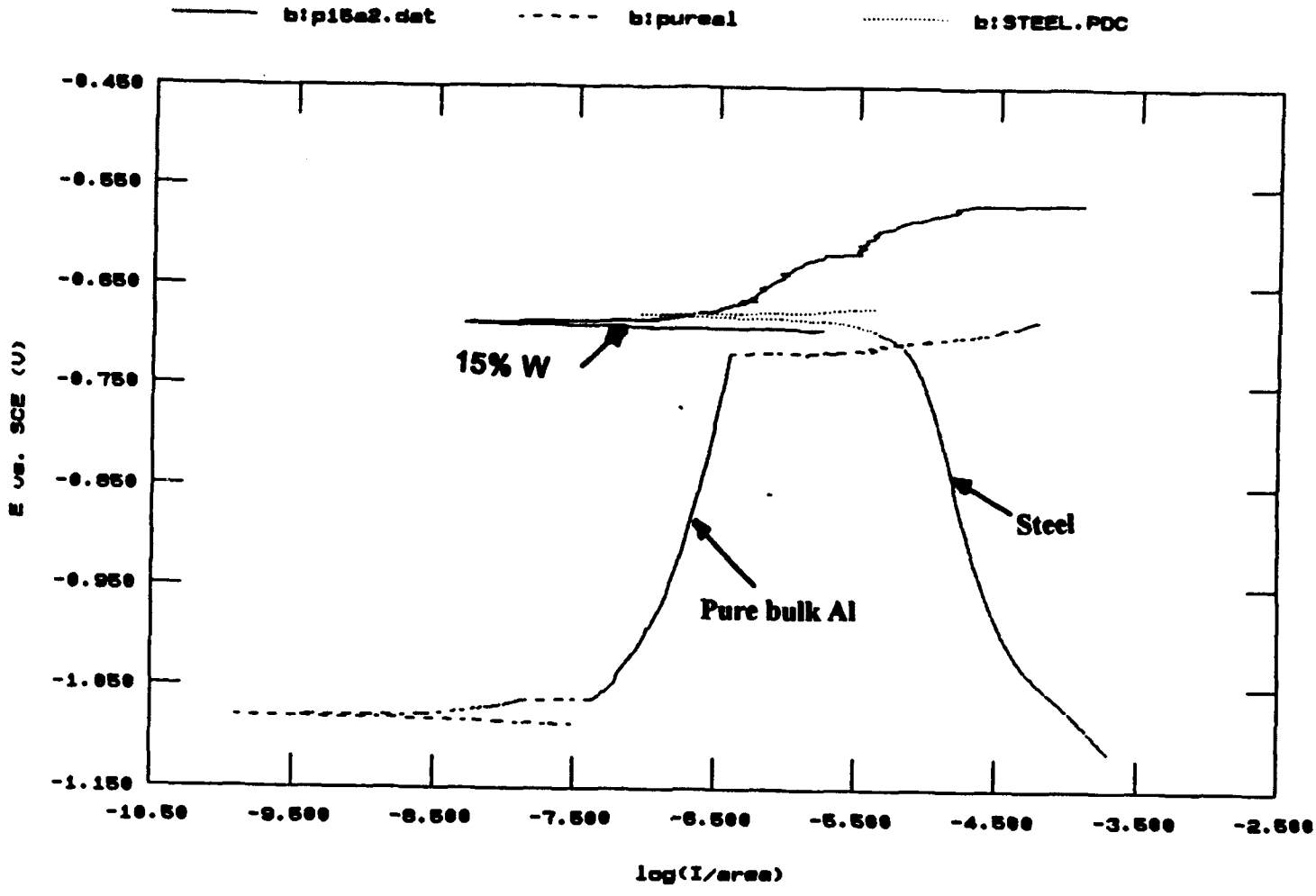


12. Anodic polarization curves of an Al15%W specimen and a pure Al specimen overlaid on the cathodic polarization curve of steel. Both scans were run in 0.1 M NaCl.

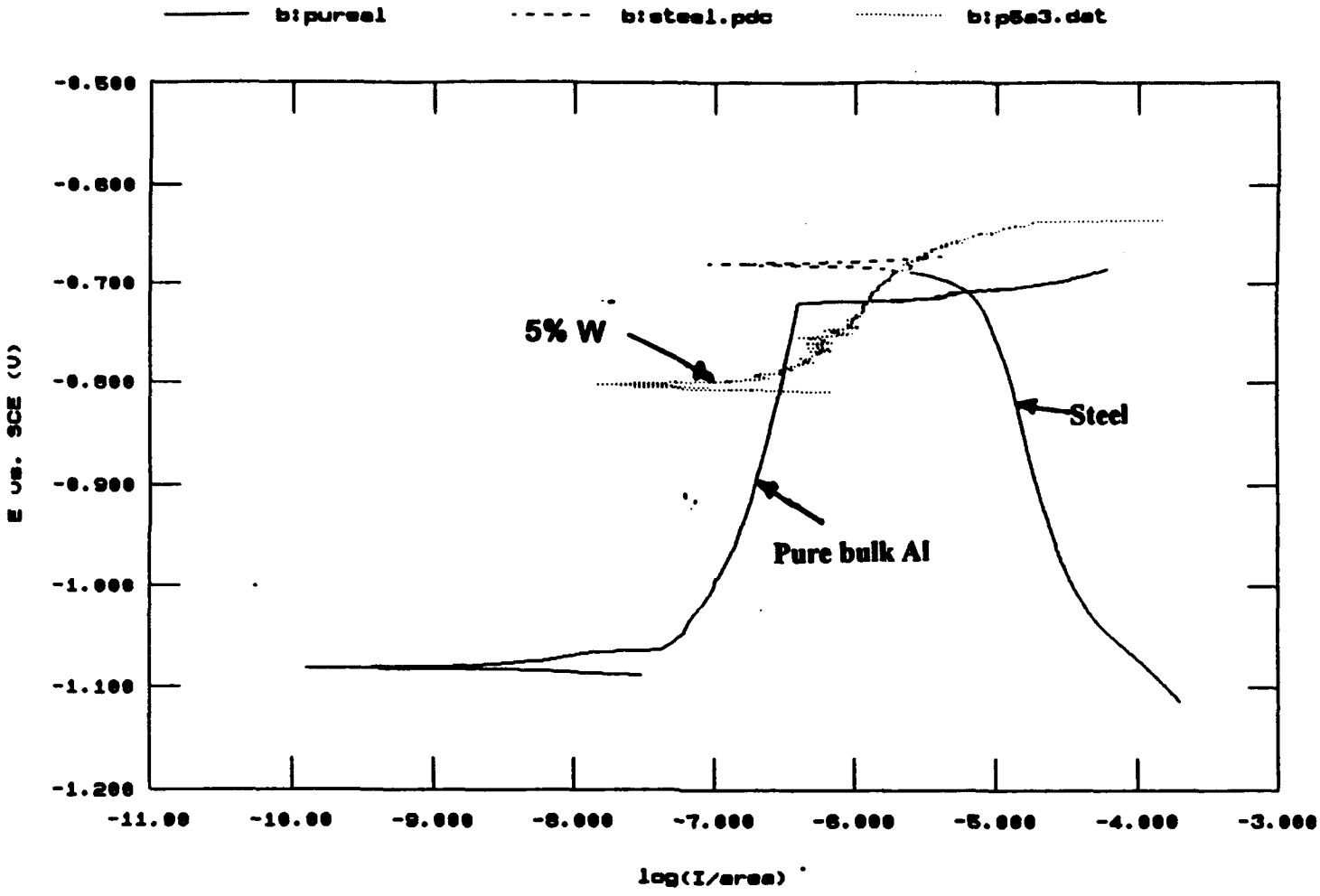


13. Anodic polarization curves of an Al5%W specimen and a pure Al specimen overlaid on the cathodic polarization curve of steel. Both scans were run in 0.1 M NaCl.

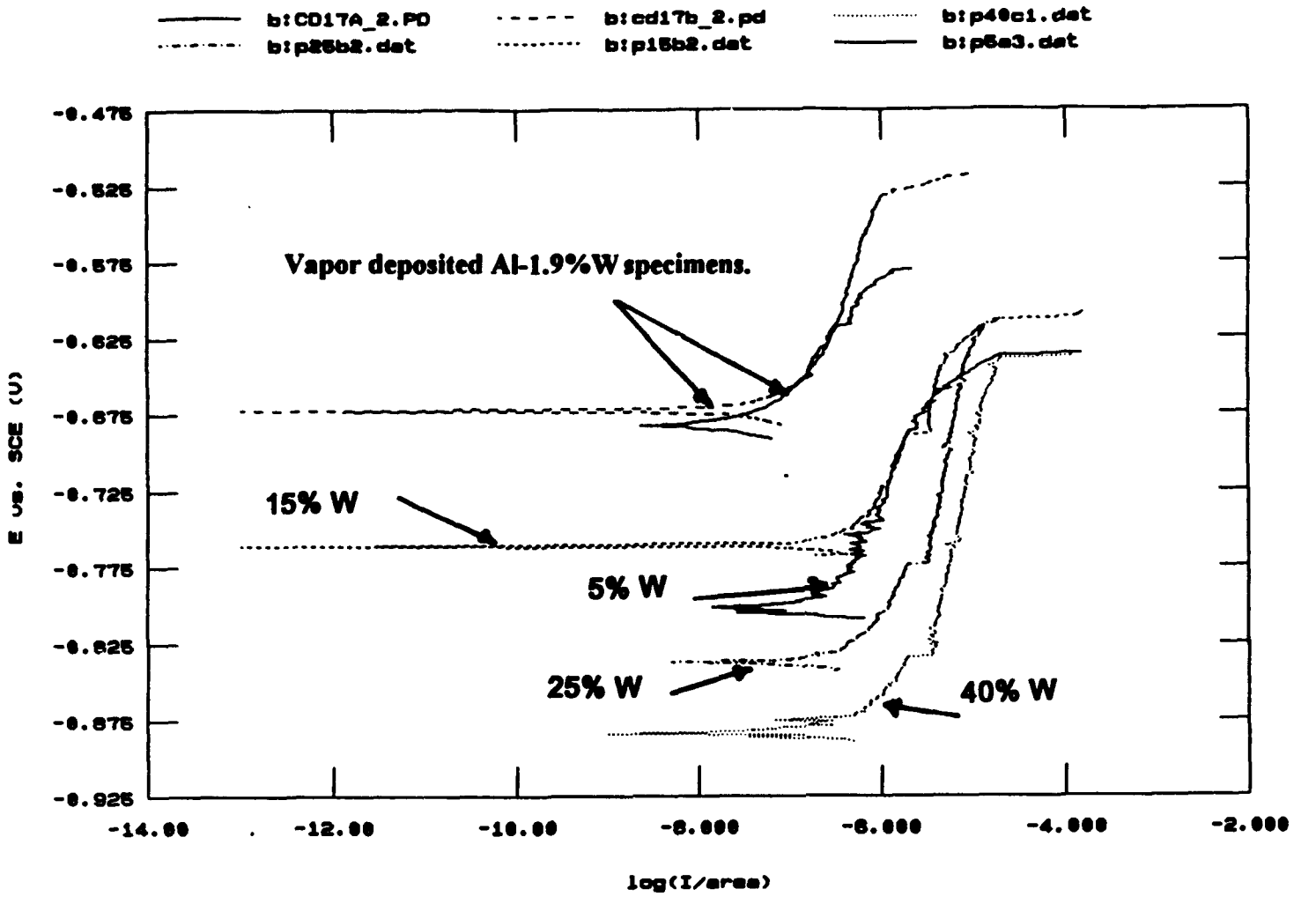


14. Anodic polarization curves of plasma sprayed Al-W specimens compared with the vapor deported Al-W specimens. All scans were run in 0.1 M NaCl at a scan rate of 0.2 mV/s and a pH of 8.0.

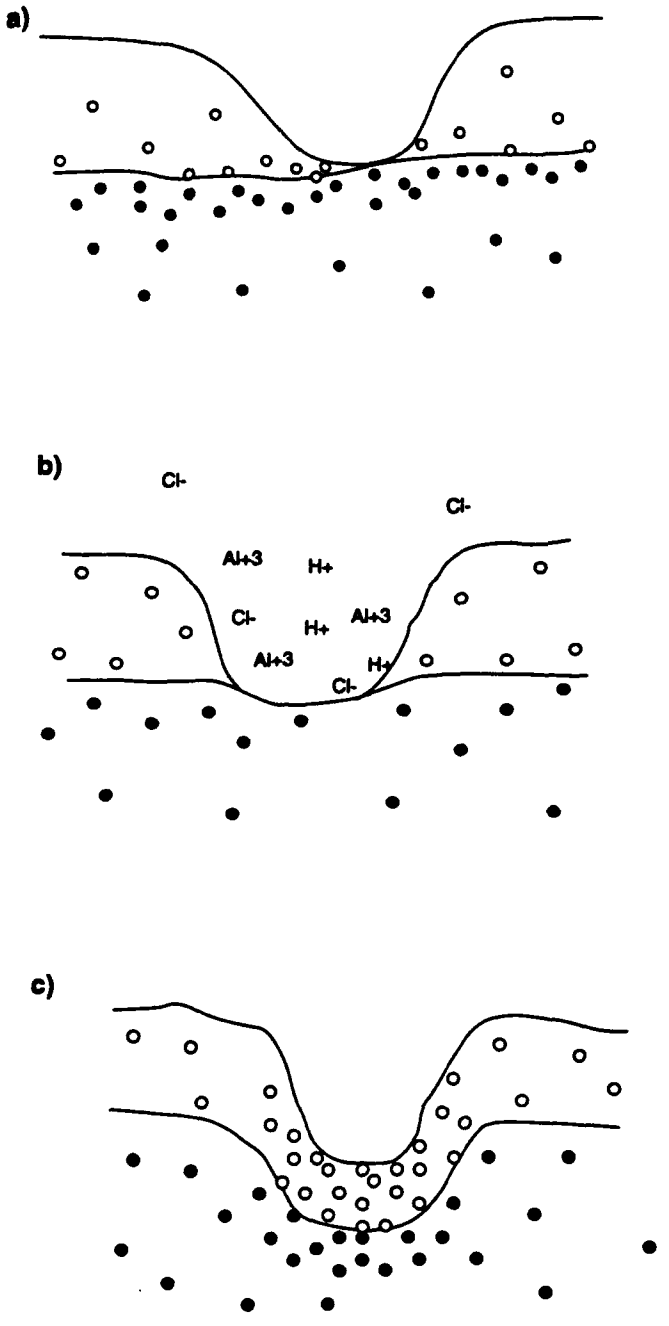


15. Schematic representation of the Solute-Rich Interphase Mechanism (SRIM). a) Solute-rich metallic region under the passive film inhibits pit formation at defects. b) Acidification of an occluded cell and dissolution of Al causes the passive film and underlying alloy to become solute-rich locally. c) Solute-rich interphase passivates the cell due to more stable film and reduced adsorption of $Cl^-$. Solid circles correspond to metallic solute; open circles correspond to oxidized solute (Ref. 9).

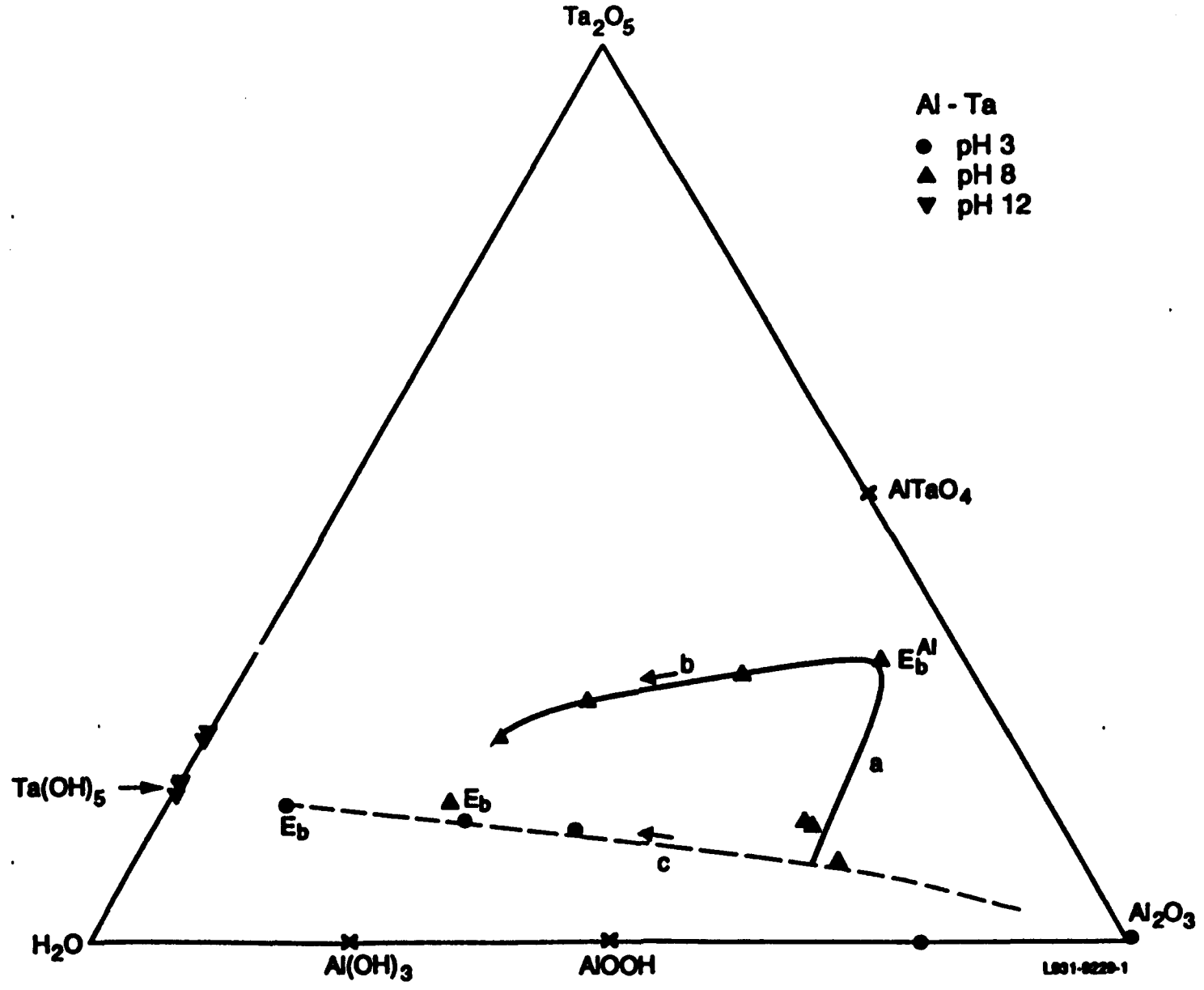


16. $Al_2O_3$-$Ta_2O_5$-$H_2O$ surface behavior diagram showing the evolution of the passive film chemistry of Al-2.8Ta during polarization in 0.1 M NaCl solutions at pH 2, 8, and 12.

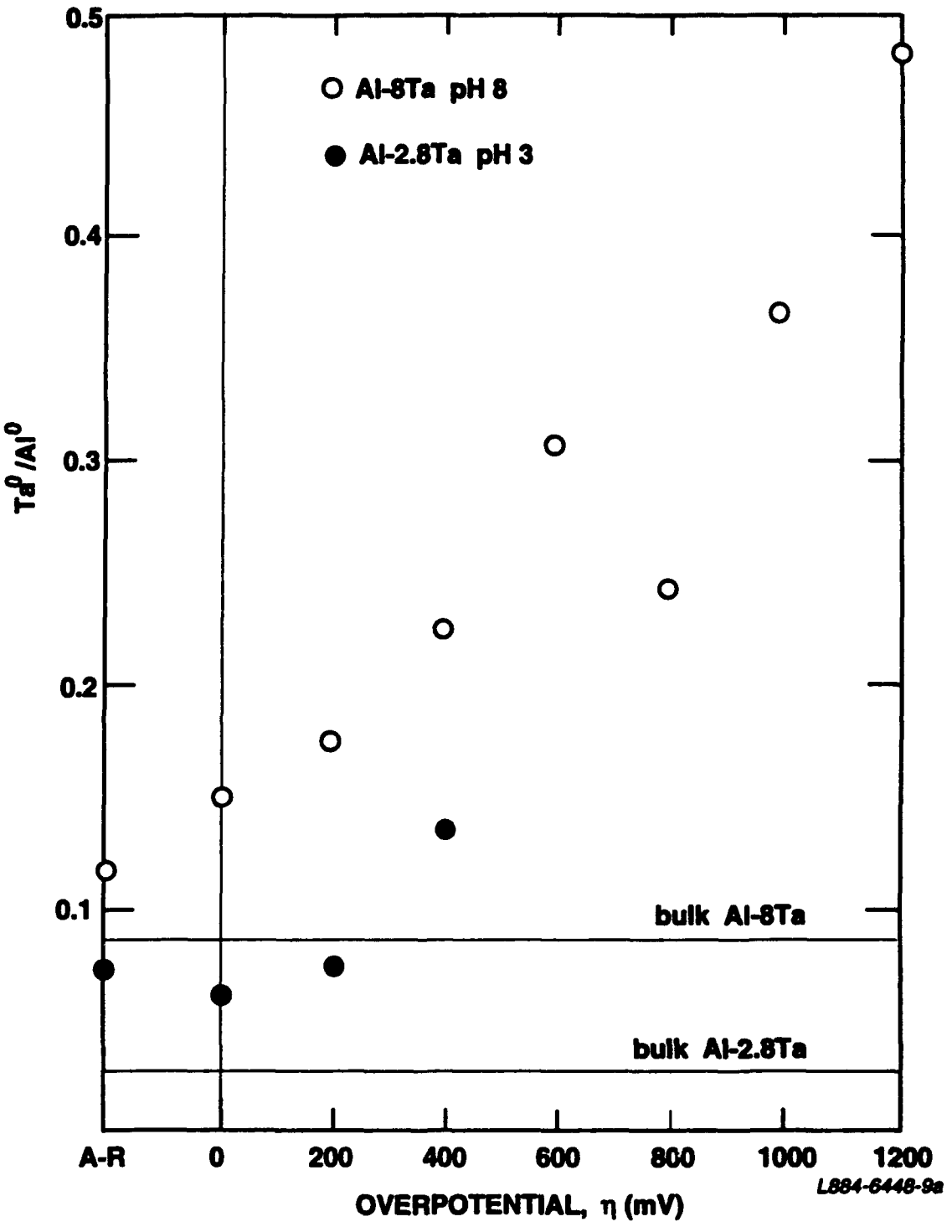


17. Ratio of metallic Ta to metallic Al as a function of overpotential for an Al-8Ta specimen polarized in a pH 8 solution [4] and an Al-2.8Ta specimen polarized in a pH 3 solution. The bulk values of the ratio are noted on the figure.